

Design and estimated performance of a new neutron guide system for the NCNR expansion project

J. C. Cook

NIST Center for Neutron Research, 100 Bureau Drive, Stop 6103, Gaithersburg, Maryland 20899-6103, USA

(Received 25 September 2008; accepted 9 January 2009; published online 11 February 2009)

An integral part of the National Institute of Standards and Technology Center for Neutron Research (NCNR) expansion project is the addition of five cold neutron guide tubes serving multiple experimental stations in an expanded guide hall. The guides have curved-straight arrangements in the horizontal plane, employing horizontally or vertically defocusing and focusing sections in some cases to improve transmission efficiency or for beam reshaping. The horizontally curved sections eliminate direct lines of sight between the source and the experimental stations, and the outer (concave) surfaces generally have higher critical angles than the inner (convex) surfaces. These features result in well-filtered cold neutron beams with no intensity losses at shorter wavelengths with respect to curved guides having the higher critical angle coatings on both surfaces. For all guides the critical angle of the outer coating of the curved section is selected to achieve a desirable characteristic wavelength, consistent with the instrument requirements. On guides where the scattering-plane beam divergence must be strictly limited, the inner radial coatings of the curved sections and the side coatings and lengths of the final straight sections are chosen to produce the desired beam divergence while the outer radial coating is selected so as to obtain a spatial-angular uniformity of the transmitted beam that is not achievable using a curved guide alone. The long-wavelength transmission of such guides tends to exceed that of equivalent straight guides using crystal filters. © 2009 American Institute of Physics. [DOI: [10.1063/1.3077144](https://doi.org/10.1063/1.3077144)]

I. INTRODUCTION

Since their inception, cold neutron sources¹ and neutron guide tubes^{2,3} (henceforth referred to simply as “guides”) have revolutionized neutron scattering research. The long wavelengths available from cold sources enable high resolution scattering measurements both at small scattering vectors and at small energy transfers. The guides allow several cm² cross-section cold neutron beams to be transported over tens of meters with minimal losses within a given angular acceptance range. This range is ultimately limited by a critical angle for total reflection θ_c that is approximately proportional to the neutron wavelength λ and is typically several millirads per angstrom in magnitude, compatible with the angular resolution tolerances and angular acceptance of many cold neutron scattering instruments. The majority of unwanted fast-epithermal neutrons and gammas emitted by the source that enter the guide do not reflect. Therefore, even the unshielded intensity of these contributions decreases rapidly with distance from the source. Consequently, guides facilitate not only the physical separation of an increased number of instruments sharing a restricted angular view of the source, but also substantially improve cold neutron signal to background ratio with little overall loss.

The NCNR expansion project provides for five new guides viewing the National Bureau of Standards Reactor’s advanced liquid hydrogen (LH₂) cold source⁴ through a 28 cm diameter beam tube. The new guides terminate in a guide hall extension adjacent to the existing facility.

II. INITIAL GUIDE DESIGN CONSIDERATIONS

The relative positions, accessibility, and neutronic requirements of the proposed instrument suite were considered prior to undertaking the detailed guide design. These instruments consist of (1) the neutron spin echo (NSE) spectrometer^{5,6} relocated from its current position on guide NG-5 to obtain a less perturbed magnetic environment on guide NG-A, (2) a new 10 m small angle neutron scattering (SANS) instrument and a 30 m SANS instrument⁷ (relocated from guide NG-3) on the split guide NG-B, (3) a variety of fundamental physics stations requiring a large, high intensity end-position beam, possibly with one or two monochromatic side beams on guide NG-C, and (4) two vertical sample reflectometers⁸ (requiring side locations) and two analytical chemistry stations [a prompt gamma activation analysis (PGAA) instrument⁹ and a neutron depth profiling instrument¹⁰] requiring a shared, small area, high capture flux end-position beam on guide NG-D. Guide NG-B, emerging from a single in-pile port, splits about a central horizontal plane. The upper and lower guides, labeled NG-Bu and NG-Bl, respectively, curve in opposite directions toward the two SANS instruments. The resulting instrument layout is illustrated in Fig. 1.

Adequate separation for five beams emerging from a beam tube of only 28 cm diameter is achieved by curving the guides initially in the horizontal plane. For all guides the curvature excludes lines of sight between the source and the guide exit, reducing or eliminating the need for crystal filters that are frequently required in straight guides. In most cases

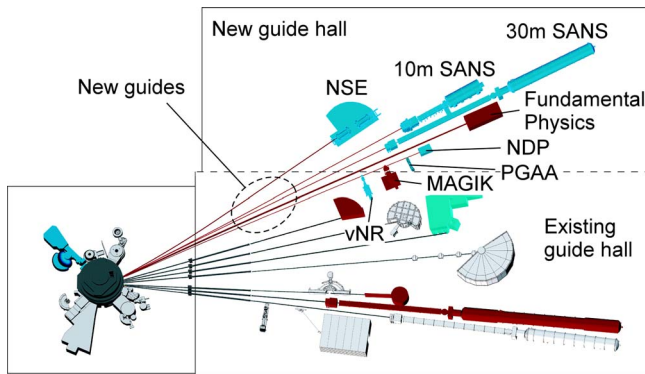


FIG. 1. (Color online) A plan view showing the new guides and the proposed instrument layout. In the guide hall areas existing guides and instruments that remain in their present locations are shown in pale gray, existing instruments that are relocated are represented in intermediate gray (blue), and new instruments are represented in dark gray (red).

the lines of sight terminate within the curved sections, well upstream of the guide exits. The in-pile guide axes project to a point near the center of the LH_2 cold source exit window. This ensures optimal guide entrance illumination both with the existing source and with a proposed future liquid deuterium (LD_2) cold source.

Curved guides have been used successfully at various neutron scattering research institutions worldwide, including the Institut Laue-Langevin¹¹ and the Laboratoire Leon Brillouin, France, ISIS at the Rutherford Appleton Laboratory, U.K., the Paul Scherrer Institute, Switzerland, FRM-II, Germany,¹² the Bragg Institute, ANSTO, Australia, the Spallation Neutron Source at Oak Ridge National Laboratory, USA, and the JRR-3M, Japan.¹³ However, one disadvantage is that curved guides produce asymmetrical spatial-angular distributions of neutrons at their exit.^{14,15} Therefore, rather than using continuous curves, the new guides are completed by long sections whose axes remain straight. The straight sections reduce the asymmetries¹⁶ and even ideally remove them under certain circumstances.¹⁷

The guide layout in Fig. 1 is possible because of supermirror developments (for which a review of the pioneering work is given in Ref. 18). Supermirrors use highly contrasting bilayer stacks^{19,20} with particular depth-graded thicknesses^{21,22} to artificially extend the total reflection angle beyond the critical angle of nickel θ_c^{Ni} (which, with the exception of beryllium, has the highest scattering length density and critical angle of the naturally occurring elements at room temperature). A supermirror is frequently characterized by the ratio m of its effective critical wave vector transfer Q_c ($\approx 4\pi\theta_c/\lambda$) to that of natural Ni Q_c^{Ni} , where $\theta_c = m\theta_c^{\text{Ni}} \approx m\gamma_{\text{Ni}}\lambda$ with $\gamma_{\text{Ni}} \approx 1.73 \text{ mrad } \text{\AA}^{-1}$. With recent developments, large area coatings with m values of 4 or more are available with sufficiently good reflectivity $R(Q)$ for use in multiple reflection devices.²³ However, because the number of bilayers increases with about the fourth power of m (Ref. 24), the challenges of limiting layer roughness (essential for high reflectivity) and curbing costs eventually lead to practical limitations on the value of m .

III. CHOICE OF SUPERMIRROR COATINGS FOR CURVED GUIDE SECTIONS

Initial estimates of the reflective coatings required for the curved guide sections were based on idealized acceptance areas,¹⁵ but without any insistence on having identical outer (concave) surface and inner (convex) surface coatings. In the following illustration, we consider only idealized “long” curved guides of constant width W and radius of curvature ρ that have sufficient length L_c to exclude direct lines of sight. “Short” curved guides with $L_c < L_{\text{LOS}}$, the line of sight distance, are treated in Ref. 25, but without distinction between the inner and outer radius coatings. Small angles and $W \ll \rho$ are assumed throughout.

The geometry of the horizontally curved guide is characterized by the coating-independent angle $\psi_c (\approx \sqrt{2W/\rho})$. The symbols $\theta_{c \text{ out}}$ and $\theta_{c \text{ in}}$ denote the critical angles of the coatings on the outer and inner radial surfaces, respectively, and m_{out} and m_{in} characterize the corresponding supermirrors. The characteristic wavelength of the curved guide λ_c is defined by

$$\lambda_c = \frac{\psi_c}{\gamma_{\text{Ni}} m_{\text{out}}} \approx \frac{1}{\gamma_{\text{Ni}} m_{\text{out}}} \left| \sqrt{\frac{2W}{\rho}} \right|, \quad (1)$$

which is the wavelength below which only trajectories undergoing garland reflections (successive reflections from the outer radius) are transmitted. Beyond the line of sight, garland reflections occur at reflection angles at the outer radius $|\chi|$ that cannot exceed a value $|\chi_{\text{max}}| = \text{MIN}(\theta_{c \text{ out}}, \psi_c)$. If ψ denotes the instantaneous trajectory angle with respect to the guide axis at a transverse position x , garland trajectories travel around parabolas described by

$$\psi^2 = \chi^2 + \psi_c^2(x/W - 1/2), \quad |\chi| \leq \text{MIN}(\theta_{c \text{ out}}, \psi_c) \quad (2)$$

bounded by $x = +W/2$ (the outer guide wall) at which point the sign of χ changes upon reflection. Such trajectories are confined within the light (green)-shaded regions of the acceptance diagrams shown in Fig. 2. [A maximum angle garland trajectory with $\chi = -\psi_c$ thereafter follows a parabola $\psi^2 = \psi_c^2(x/W + 1/2)$ that just grazes the inner wall—see dashed black line in Fig. 2(a)].

When $\lambda \leq \lambda_c$, the area within the parabola [Fig. 2(a)] is proportional to λ^3 . Therefore, with decreasing wavelength below λ_c , the guide transmission falls rapidly, the spatial distribution of the transmitted beam is increasingly biased toward the outer radius, and the beam divergence has a width that is correlated with transverse position x . For these reasons it is most desirable to decrease λ_c below the minimum instrument operating wavelength, while still benefitting from the rapid filtering effect for $\lambda < \lambda_c$. Evidently from Eq. (1) m_{out} must vary proportionally to $1/\sqrt{\rho}$ in order to achieve a given λ_c .

When $\lambda > \lambda_c$, zigzag reflections are possible for transmitted neutrons. With increasing wavelength above λ_c , the zigzag trajectory fraction [within the dark (blue)-shaded regions in Figs. 2(b) and 2(c)] increases and the spatial-angular distributions of the transmitted beam become more symmet-

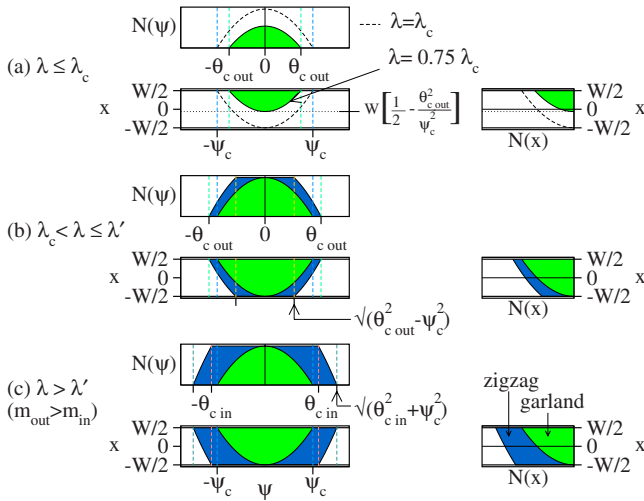


FIG. 2. (Color online) Two-dimensional acceptance areas for idealized long ($L_c \geq L_{LOS}$) curved guides at three wavelengths (transverse position x vs trajectory angle ψ). Also shown are the corresponding angular and spatial distributions at the guide exit, $N(\psi)$ and $N(x)$, assuming perfect reflectivity and uniform guide entrance illumination. (a) For $\lambda \leq \lambda_c$ (the equality is represented by the dashed black curve), transmission occurs only via garland reflections [within the light (green) shaded regions]. (b) and (c) are for $\lambda_c < \lambda \leq \lambda'$ and $\lambda > \lambda'$, respectively, where zigzag reflections [within the dark (blue) shaded regions] are possible. In (b) the divergence is limited by the outer radius coating to lie within $\pm \theta_{c\ out}$ and $\pm \sqrt{(\theta_{c\ out}^2 - \psi_c^2)}$ at the outer and inner radii respectively. In (c), possible only when $\theta_{c\ in} < \theta_{c\ out}$, the divergence is limited by the inner radius coating to lie within $\pm \sqrt{(\theta_{c\ in}^2 + \psi_c^2)}$ and $\pm \theta_{c\ in}$ at the outer and inner radii, respectively.

ric. The angular limits of the acceptance area for $\lambda > \lambda_c$ are given by Eq. (2) but with $\chi^2 = \chi_{\max}^2 = \text{MIN}(\theta_{c\ in}^2 + \psi_c^2, \theta_{c\ out}^2)$, i.e.,

$$\psi_{\max}^2 = \text{MIN}(\theta_{c\ in}^2 + \psi_c^2, \theta_{c\ out}^2) + \psi_c^2(x/W - 1/2) \quad \lambda > \lambda_c. \quad (3)$$

When $\theta_{c\ in} \geq \theta_{c\ out}$, the first term on the right hand side of Eq. (3) is always $\theta_{c\ out}^2$; consequently $|\psi|$ at the inner radius ($x = -W/2$) is always less than $\theta_{c\ in}$ [Fig. 2(b)] and the acceptance area asymptotically approaches that of an unfiltered straight guide of equal width with coatings m_{out} in the long wavelength limit. However, when $\theta_{c\ in} < \theta_{c\ out}$, the cross over defined by the MIN function in Eq. (3) occurs at a finite wavelength λ' given by

$$\lambda' = \frac{m_{\text{out}}}{\sqrt{(m_{\text{out}}^2 - m_{\text{in}}^2)}} \lambda_c. \quad (4)$$

Therefore, for all $\lambda > \lambda'$, Eq. (3) becomes

$$\psi_{\max}^2 = \theta_{c\ in}^2 + \psi_c^2(x/W + 1/2) \quad \lambda > \lambda', \quad (5)$$

where clearly $|\psi_{\max}|$ at the inner radius ($x = -W/2$) is equal to $\theta_{c\ in}$, increasing monotonically with increasing x to a value $\sqrt{\theta_{c\ in}^2 + \psi_c^2}$ (which is less than $\theta_{c\ out}$) at the outer radius. Therefore, λ' is the wavelength above which the transmission becomes limited by $\theta_{c\ in}$ rather than by $\theta_{c\ out}$. Such a scenario is represented in Fig. 2(c).

The relationship between λ' and λ_c is illustrated in Fig. 3. Equation (1) shows that λ_c is independent of m_{in} . Equation (4) shows that λ' diverges as $m_{\text{in}} \rightarrow m_{\text{out}}$, and that $\lambda' \rightarrow \lambda_c$ for $m_{\text{out}} \gg m_{\text{in}}$. Of course, for $\lambda < \lambda_c$, the transmission is indepen-

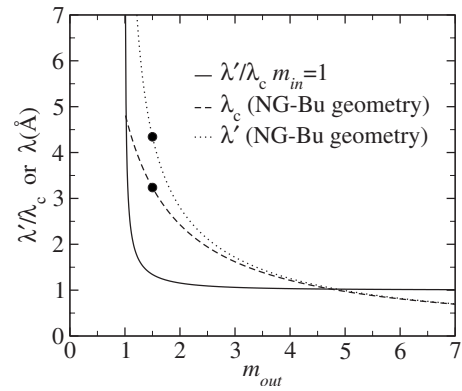


FIG. 3. The solid curve shows the ratio of λ' to λ_c for an ideal long curved guide as a function of m_{out} for a case where $m_{\text{in}}=1$. One such example is provided by the SANS guide NG-Bu, where the value of m_{out} is chosen to reduce λ' toward (and hence λ_c below) the minimum operating wavelength. The significance of λ' is explained in the text. The dashed and dotted curves are loci of λ_c and λ' , respectively, for a long curved guide that has W/ρ equivalent to that of guide NG-Bu. The circles indicate the specific values obtained for NG-Bu by choosing $m_{\text{out}}=1.5$, at which point $\lambda'/\lambda_c \approx 1.34$.

dent of m_{in} . Therefore, an instrument on a long curved guide with $\theta_{c\ in} < \theta_{c\ out}$ ideally incurs no losses with respect to one with $\theta_{c\ in} = \theta_{c\ out}$ when $\theta_{c\ in}$ is chosen so as to retain λ' above the maximum instrument wavelength. Conversely, if the instrument is operated in the range $\lambda \geq \lambda'$, the choice of $\theta_{c\ in}$ limits the transmission. This apparent loss is incurred intentionally in the so-called “phase space tailoring” (PST) guides (see Ref. 17) in order to produce ideally uniform spatial-angular distributions with optimal intensity for all $\lambda \geq \lambda'$. In this particular case, λ' is set toward the *minimum* rather than the maximum instrument wavelength. PST guides are useful for instruments requiring low-to-moderate beam divergence. They consist of a line-of-sight-excluding curved section, followed by a straight section. The straight section defines the beam divergence by suitable choices of its side coating critical angle $\theta_{c\ str}$ and its length L_{str} . Specifically, the divergence will not to exceed $\pm \theta_{c\ str}$ for all wavelengths greater than the minimum instrument operating wavelength λ_{min} , provided that the minimum straight guide length satisfies

$$L_{\text{str}} \geq W/\theta_{c\ str}(\lambda_{\text{min}}). \quad (6)$$

If Eq. (6) is satisfied, the output of the straight guide is ideally uniform and optimal in intensity for all $\lambda > \lambda_{\text{min}}$ if its entrance is uniformly illuminated by the preceding curved guide for this wavelength range. In order to achieve this, it makes most sense to match $\theta_{c\ in}$ to $\theta_{c\ str}$ then increase $\theta_{c\ out}$ until λ' falls below λ_{min} [note that this also requires $\lambda_c < \lambda_{\text{min}}$ —see Eq. (4)]. If $\lambda' \leq \lambda_{\text{min}}$, the divergence at the inner radius of the curved guide exit $|\psi_{\max}(-W/2)|$ is fixed at $\theta_{c\ in}$ ($=\theta_{c\ str}$) [see Fig. 2(c)], guaranteeing full illumination for the whole wavelength range. Contrary to straight guides with crystal filters, where some attenuation of the useful wavelength range is inevitable, the PST guide ideally rejects only unwanted neutrons exiting the curve that have $|\psi| > \theta_{c\ str}$. The only price paid for the potentially superior performance of the PST guide is that related to increasing $\theta_{c\ out}$ sufficiently, together with any consequent reduction in reflectivity.

TABLE I. Guide parameters and predicted wavelengths above which the neutron transmission becomes “collimation limited” rather than critical angle limited for guides NG-A and NG-5 for the specific case of $L_{gs}=3.5$ m and $w_s=h_s=4$ cm.

Guide	w_g/cm	h_g/cm	m_h	m_v	Horizontal plane transmission collimation limited for $\lambda(\text{\AA})$ greater than	Vertical plane transmission collimation limited for $\lambda(\text{\AA})$ greater than
NG-A	5	7	1.2	1.8	6.2	5.0
NG-5 optical filter	3.5	7	≈ 1.18 (^{58}Ni)	≈ 1.18 (^{58}Ni)	5.2	7.7

The curved sections for the new guides are polygonal approximations to ideal curves, formed by straight elements placed tangent to a circle. The discrete change in angle between elements produces disallowed regions within the ideally allowed phase space region with saw-toothlike modulations of the ideally parabolic envelopes described by Eq. (3) or Eq. (2) with $|\chi|=\chi_{\max}$. The severity of these features diminishes with decreasing element length to radius of curvature ratio and the negative performance impact is slight for the new guides that use 0.5 m long elements in the curved sections.

IV. USE OF MONTE CARLO SIMULATIONS

Acceptance diagrams are helpful for establishing initial guide designs and determining absolute phase space boundaries. Using them, however, to obtain reliable performance predictions under the nonidealized illumination and reflectivity conditions that usually occur is difficult. Some efforts have been made for fully illuminated curved guides with constant fractional reflectivity $R(Q < Q_c) < 1$,^{26–29} but the complex correlations involved in more realistic situations are much more readily solved by Monte Carlo (MC) simulation. An updated version of the author’s own code used in previous studies³⁰ is used for the simulations presented here.

The MC geometry assumes that neutrons are emitted only from the elliptically shaped exit window of the LH₂ source, having determined that trajectories starting outside of this region usually have low transmission probability with little impact on the simulation results (apart from decreasing calculation efficiency). Nonetheless, all guide optimizations incorporate sufficient margins so as to benefit from (i) plausible improvements in reflectivity over the assumed models and (ii) a more extensive source region anticipated from a LD₂ cold source [for which the MC source was developed from a MCNP (Ref. 31) prototype model³²].

V. DESIGN FOR PHASE SPACE TAILORING GUIDES NG-A AND NG-B

Guides NG-A and NG-B deliver beams to the NSE and the SANS instruments, respectively. Their design goal is to maximize intensity within a low divergence beam in the scattering plane with a high degree of spatial-angular uniformity. This is achieved by using high R , low m coatings without focusing, and the PST guide concept (see Sec. III).

For PST guides we recall that it is desirable to shift not only λ_c but also λ' below the minimum instrument operating wavelength. For small area, low divergence guides, significant under-illumination effects are shifted to long wavelengths and the simulations indicate that despite nonideali-

ties, a high degree of phase space symmetry is to be anticipated for the entire instrument ranges. Equation (6) is also readily satisfied for these guides with L_{str} typically several times greater than the minimum necessary.

For NG-A, a strong initial curvature ($\rho \approx 151$ m) is required to achieve adequate clearance between the NSE instrument and the 10 m SANS guide NG-BI (see Fig. 1). This value of ρ requires a high value of m_{out} ($=3.6$) to reduce λ_c toward the minimum operating wavelength [$\lambda_c=4.14$ \AA —see Eq. (1)]. The relatively low value of m_{in} ($=m_{\text{str}}=1.2$) that defines the horizontal beam divergence causes λ' ($=4.39$ \AA) to approach λ_c [see Eq. (4)] as required for good short wavelength performance of the PST guide.

The initial 5 cm wide \times 12 cm guide height is reduced to 5×7 cm² downstream of the velocity selector (about the maximum beam size compatible with the latter). Beyond the guide exit, the beam drifts approximately 3.5 m through the first NSE solenoid to the sample. At short wavelengths the beam divergence at the sample is limited by the guide coatings, whereas at long wavelengths it is limited by the natural collimation created by the guide exit width and height w_g and h_g , respectively, and the sample width and height w_s and h_s , respectively. The transition between the two regimes occurs when

$$\lambda = \frac{w_g + w_s}{2m_h \gamma_{\text{Ni}} L_{gs}} (\text{horizontal plane})$$

$$\text{or } \frac{h_g + h_s}{2m_v \gamma_{\text{Ni}} L_{gs}} (\text{vertical plane}), \quad (7)$$

where L_{gs} is the guide exit-sample separation and m_h and m_v define the side and top/bottom critical angles of the final straight guide sections, respectively. Table I compares the transition wavelengths and related parameters for guide NG-A with the existing NG-5 optical filter, assuming that the NSE instrument has $L_{gs}=3.5$ m with a 4 cm² sample.

Because the final beam heights of NG-A and NG-5 are identical (7 cm), the vertical angular distributions of neutrons reaching a 4×4 cm² sample are practically identical when collimation limited for both guides (i.e., for all $\lambda \geq 7.7$ \AA). The increased NG-A vertical (out-of-scattering-plane) divergence for all $\lambda < 7.7$ \AA due to the higher m top/bottom coating (see Table I) leads to increased intensity on the sample. Horizontally, the NG-A and NG-5 critical angles are similar but the guide widths are different. Therefore, for $\lambda \leq 5.2$ \AA (critical angle limited for both guides), the angular distribution widths are almost identical, but the NG-A distribution exhibits a less pronounced structure. For $\lambda \geq 6.2$ \AA (collimation limited for both guides), the standard deviations of the approximately triangular angular distributions are about 19%

TABLE II. Some parameters of the SANS instrument PST guides NG-BI and NG-Bu. Both guides have 5×5 cm² interior dimensions.

Guide	ρ/m	m_{out}	m_{in}	$\lambda_c/\text{\AA}$	$\lambda'/\text{\AA}$
NG-BI	781	1.65	1	3.97	4.99
NG-Bu	1432	1.5	1	3.22	4.32

greater for NG-A than for NG-5 due to the increased guide width. This is close to the predicted increase of 20% [i.e., $(w_g + w_s)_{\text{NG-A}} / (w_g + w_s)_{\text{NG-5}}$] if the distributions were exactly triangular.

For the 10 m SANS (operating most frequently in the 6 Å wavelength range) and the 30 m SANS (operating in the 5–15 Å range), the respective PST guides NG-BI and NG-Bu have the characteristics summarized in Table II. Because high reflectivity, natural nickel coatings are used on all surfaces (except the outer radii of the curved sections), the 45–49 m long guides preceding the velocity selectors are expected to have very good transmission, despite the relatively small interior guide dimensions. For example, even at $\lambda = 10$ Å, the simulated transmission efficiencies are between 72% and 75% of their perfect reflectivity values.

VI. DESIGNS FOR “HIGH FLUX” GUIDES NG-C AND NG-D

These guides deliver beams to instruments that can exploit the increased beam divergence from focusing guides with high m supermirrors. The initial curved sections of guides NG-C and NG-D expand the beam widths from 5 cm to 11 cm and from 3 cm to 6 cm, respectively. Therefore the curved guide quantities (λ_c , λ' , etc.) refer to the constant width parts of the curve. For both guides m_{out} is increased (λ_c is decreased) in order to enhance shorter wavelength transmission around the bend. This is performed more aggressively for NG-C ($\rho \approx 933$ m, $m_{\text{out}} = 3.6$, $\lambda_c \approx 2.47$ Å) than for NG-D ($\rho \approx 907$ m, $m_{\text{out}} = 2.0$, $\lambda_c \approx 3.33$ Å). For NG-D a compromise is struck between (i) approaching optimum end-position capture flux for the chemistry stations and optimum $\lambda \approx 4.5$ –5 Å flux for the reflectometers (favoring reduced λ_c) and (ii) filtering epithermal neutrons and minimizing higher order Bragg-reflected intensity from the reflectometer monochromators (favoring increased λ_c). In contrast with the PST guides, the inner radii and straight guide side coatings are adjusted to approach maximum flux in the most cost-effective manner rather than to achieve a specific beam divergence. Ideally, this suggests setting λ' just above the maximum operating wavelengths (see Sec. III) or into a spectral region where the source intensity is low. However, the simulations reveal that λ' can be reduced to significantly shorter wavelengths due to (i) effects of underillumination caused by the restricted angular limits of the elliptical source and (ii) a natural bias against large-angle trajectory transmission that compounds, as Q increases, by the combination of increasing reflection numbers and diminishing $R(Q)$. For example, for NG-C it is found that increasing m_{in} and m_{str} above about 2.4 (despite the large value of $m_{\text{out}} = 3.6$) benefits only the transmission of neutrons with wavelengths below about 5 Å. Furthermore, as $\lambda \rightarrow 5$ Å, these additional neu-

trons are emitted increasingly toward the source perimeter where trajectories have lower transmission probability for the reasons just stated. In fact, because the reflectivity at a given $Q < Q_c$ tends to decrease slightly as m increases, potential transmission gains from increasing Q_c may be nullified or negated by a poorer average reflectivity. For wavelengths greater than about 5 Å the horizontal divergence at the NG-C guide exit saturates at about ± 23 mrad. This value may be deduced approximately from the angle between the extreme source edge and the opposing edge of the in-pile guide entrance port ($\approx \pm 50$ mrad), transformed by the effect of the guide width expansion from 5 to 11 cm. This transformation ideally reduces the entrance divergence by a factor 5/11 (i.e., to about ± 23 mrad at the exit), as dictated by Liouville’s theorem.

Although geometry restrictions cause underillumination, so-called “ballistic” guides³³ can reduce reflection losses, allowing higher m supermirrors to be usefully exploited. Typical ballistic configurations include linear taper-straight-linear taper, parabolic straight parabolic, or elliptical.^{34–37} These profiles transform a small, divergent, high flux beam at the source into a larger, less divergent, lower flux beam for the majority of the guide length, then back into a smaller, more divergent, higher flux beam at the exit. The transformation reduces the mean number of reflections ($\langle n \rangle$) required for transmission and the decreased divergence in the main (longest) part of the guide means that reduced m , increased R coatings may also be used in this section. With fewer reflections and improved average reflectivity, the ballistic guide increases the transmission efficiency. The parabolic and elliptical profiles have the advantage of producing beam foci beyond the guide ends, favoring displaced sources and samples. They also smooth the angular transitions between their end sections and the central section, increasing the acceptance area for a broader wavelength range.³⁸ Despite the increased coated area, the ballistic guide cost is somewhat offset by the use of lower m supermirrors over the majority of its length.

Figure 4(a) shows a projection of the quasielliptical vertical profile of guide NG-C. At most wavelengths of interest, the mean number of top/bottom reflections ($\langle n_v \rangle$) is reduced by roughly a factor of 2 with respect to an equivalently coated guide of constant height of 11 cm [see Fig. 4(b)]. The peak flux is obtained about 1 m beyond the guide exit. The end position of this guide favors experiments requiring high capture flux and maximum throughput (total neutrons per second) within the requested 11×11 cm² beam area. Despite the enhanced vertical divergence, the horizontal divergence is moderated by the overall expansion of the beam width and by the saturation mentioned above. The initial horizontal guide profile consists of discrete, linearly tapered guide elements whose surfaces would be approximately tangent to a parabola at their midpoints if the guide axis were straight; however, each element is angularly displaced with respect to the preceding one so as to lie along the required curvature.

The end station on guide NG-D requires small area, high capture flux beams. Ballistic profiles are used horizontally and vertically. The first sections expand the beam horizontally along a similar principle to that just described for guide

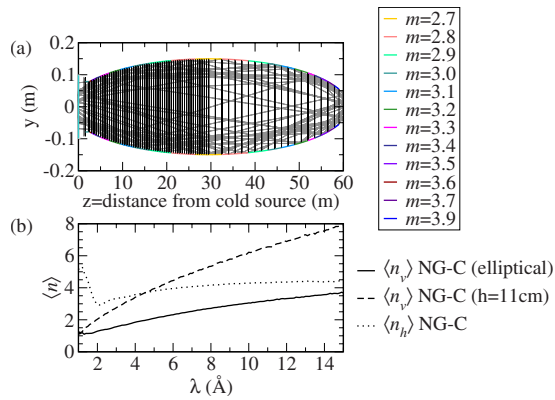


FIG. 4. (Color online) (a) Schematic projection of the quasielliptical vertical profile of NG-C showing a random sample of transmitted 4 Å neutron trajectories that make at least one reflection. The majority requires at most one or two upper/lower reflections for transmission. For clarity, trajectories transmitted with no reflections are omitted. With the foci of the ellipse beyond each end of the guide, one identifies trajectories originating close to the source focus that make only a single reflection (as expected). Supermirror m values are distinguished by shade/color. Note that higher m is needed near the entrance and exit where the taper angles and beam divergence are greatest. The supermirror selection shown performs equivalently to a blanket coating with $m=3.9$ but is significantly more cost effective. (b) Shows the simulated mean number reflections for transmitted neutrons, $\langle n \rangle$, as a function of λ . The bold curve is for upper/lower surface reflections $\langle n_v \rangle$ from the elliptical guide compared with an equivalently coated 11 cm high guide (dashed curve). The dotted curve is the mean number of side reflections $\langle n_h \rangle$. For idealized, horizontally curved guides, $\langle n_h \rangle$ is minimized at $\lambda = \lambda_c$ (Ref. 6). For NG-C the minimum in $\langle n_h \rangle$ is located at shorter wavelength due to the expanding initial portion of the curve and imperfect reflectivity. The long-wavelength increase in $\langle n_h \rangle$ is slow because (i) the divergence is limited by $\theta_{c, \text{in}}$ for $\lambda > \lambda'$ (≈ 3.31 Å) and (ii) the divergence “saturates” due to underillumination and reflectivity losses.

NG-C, and the initial vertically expanding profile is approximately parabolic. The expanded beam height and width reduce on approach to the reflectometers, consistent with the monochromator dimensions. The enhanced horizontal beam divergence caused by the horizontal focusing increases $\Delta\lambda/\lambda$ for the reflectometers at the expense of a tolerable (and relatively minor) loss in Q -resolution. When using larger horizontal mosaic spread monochromators the larger beam divergence broadens the Bragg-reflected phase space in the region that is accepted by the reflectometer slits, improving both the intensity on sample and signal-to-background ratio. Downstream of the reflectometers the horizontal and vertical focusing continues, further compressing the beam dimensions and increasing the end-position flux. Higher m supermirrors are used toward the end of the guide to compensate for the growing divergence as the beam propagates through the taper.

VII. RESULTS AND DISCUSSION

The majority of the following simulations assume supermirror reflectivities considered to resemble those on superpolished³⁹ Borkron® glass with rms surface roughness $\sqrt{\langle u^2 \rangle}$ of 0.7 nm.^{40,41} Example models are shown in Fig. 5. Even for low m supermirror coatings where the number of deposited bilayers is relatively small, the depth-graded supermirror d -spacing is expected to resemble that prescribed by Ref. 22. In this way the structured reflectivity beyond the

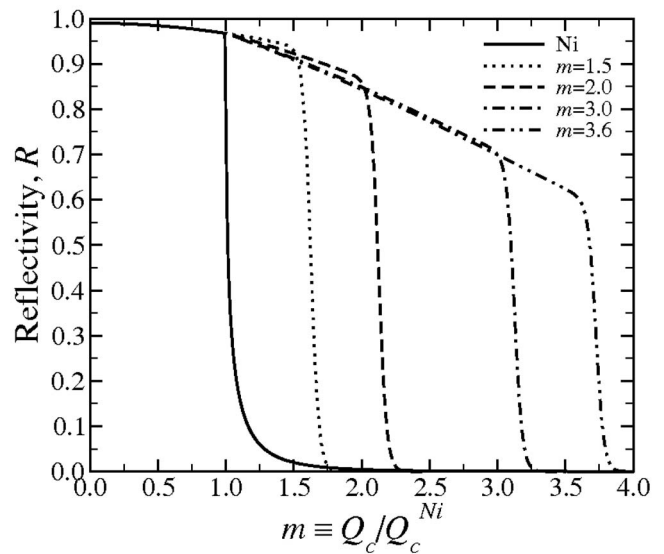


FIG. 5. Supermirror reflectivity models approximating to typical supermirror performance on substrates with a rms surface roughness $\sqrt{\langle u^2 \rangle}$ of 0.7 nm. For these supermirror models, m defines the Q value near the summit of the rapid downturn of R . The curves are dotted: $m=1.5$, dashed: $m=2$, dot-dashed: $m=3$, and dot-to-dashed: $m=3.6$. For comparison, a Ni coating reflectivity (bold curve), based on Fresnel’s law is also shown. In each case, the effect of surface roughness on the reflectivity is approximated by an $\exp(-Q^2\langle u^2 \rangle)$ Q -dependence.

supermirror regime is reduced with respect to a mirror composed of periodic bilayers⁴² to an extent where its impact on the short wavelength transmission and angular distributions of the transmitted neutrons is negligible for these guides. For ideal, long curved guides, flux gains from improved $R(Q)$ favor both short and long wavelengths because $\langle n_h \rangle$ is minimized near $\lambda = \lambda_c$ and diverges as $\lambda \rightarrow 0$. For nonidealized guides the wavelength dependence of the gain is complex due to correlations between the reflection angle and $R(Q)$ and due to underillumination when the mean reflection angle $\langle \theta \rangle$ corresponds to a decreasing value of Q as λ increases.

Effects of several sources of random imperfections are investigated. The intrinsic waviness of the glass [which is expected to be about 10^{-4} rads full width at half maximum (FWHM) for polished glass or selected float glass] contributes the least significant losses when calculated using a similar method to that described in Ref. 43. The largest integrated flux losses due to waviness are about 0.8% for the SANS guides, NG-Bu and NG-BI, about 0.1% for guide NG-A, and are almost insignificant for guides NG-C and NG-D. Additional effects investigated include (i) fractional variations $\Delta m/m$ of the supermirror m values with respect to the nominal values, (ii) element-to-element horizontal and vertical plane angular misalignments, and (iii) element-to-element lateral shift misalignments. The imperfections were generated from Gaussian distributions of specified FWHM symmetrically about the nominal values. Perhaps slightly pessimistic FWHM values of 0.1, 1.5×10^{-4} rad, and 0.03 mm were chosen for (i), (ii), and (iii), respectively. Because each randomly perturbed configuration is unique, estimates of the effects of these perturbations were obtained by averaging over 20 simulations for each guide.

TABLE III. Integrated quantities obtained from MC simulations. The simulation details are summarized in the left hand column. There are five entries in each cell containing a numerical quantity. The first four entries [rows (a)–(d)] relate to the new guide described in the first entry of the corresponding left hand column; the fifth entry [row (e)] is the reference simulation for the existing facility [with the existing (unit 2) LH₂ cold source model] as described by the second entry of the corresponding left hand column. The conditions for the first four entries break down as follows: (a) LH₂ cold source model, all random imperfections described in the text (average over 20 simulations), nominal m values, and 0.7 nm rms roughness; (b) LH₂ cold source model, negligible guide misalignments, nominal m values, and 0.7 nm rms. roughness; (c) as for (b) but with 0.5 nm rms. roughness; and (d) as for (b) but using a model for a future LD₂ cold source. The MC statistical errors do not exceed those implied by the number of quoted significant figures and, for some values, are significantly smaller. Systematic uncertainties caused by typical misalignments and variations in $R(Q)$ generally exceed the statistical errors, as implied by the spread between the three quoted values in (a), (b), and (c), or by examination of Fig. 6 to Fig. 9.

Guide/position	Phase space tailoring?	Capture (thermal equivalent)		Integrated flux, φ_{int} (cm ⁻² s ⁻¹)	Neutrons/s	Mean wavelength (Å) $\langle \lambda \rangle \approx 1.8\varphi_c / \varphi_{\text{int}}$
		flux, φ_c (cm ⁻² s ⁻¹)				
NG-A NSE on 4×4 cm ² sample (polarizer replaced by regular guide section)	Yes	(a) 7.69×10 ⁸		2.37×10 ⁸	3.78×10 ⁹	5.84
		(b) 7.90×10 ⁸		2.45×10 ⁸	3.91×10 ⁹	5.81
		(c) 9.06×10 ⁸		2.90×10 ⁸	4.63×10 ⁹	5.63
		(d) 1.38×10 ⁹		3.98×10 ⁸	6.36×10 ⁹	6.24
		(e) 7.67×10 ⁸		2.53×10 ⁸	4.05×10 ⁹	5.46
NG-5 NSE on 4×4 cm ² sample (polarizer replaced by regular guide section)	No					
NG-BI (10 m SANS) at velocity selector entrance	Yes	(a) 2.06×10 ⁹		5.47×10 ⁸	1.37×10 ¹⁰	6.76
		(b) 2.20×10 ⁹		5.89×10 ⁸	1.47×10 ¹⁰	6.70
		(c) 2.36×10 ⁹		6.31×10 ⁸	1.58×10 ¹⁰	6.73
		(d) 4.11×10 ⁹		9.81×10 ⁸	2.45×10 ¹⁰	7.53
		(e) 1.49×10 ⁹		3.85×10 ⁸	9.62×10 ⁹	6.95
NG-7 SANS at velocity selector entrance	No					
NG-Bu (30 m SANS) at velocity selector entrance	Yes	(a) 2.22×10 ⁹		6.14×10 ⁸	1.54×10 ¹⁰	6.49
		(b) 2.35×10 ⁹		6.55×10 ⁸	1.64×10 ¹⁰	6.44
		(c) 2.50×10 ⁹		6.91×10 ⁸	1.73×10 ¹⁰	6.49
		(d) 4.35×10 ⁹		1.07×10 ⁹	2.67×10 ¹⁰	7.32
		(e) 1.49×10 ⁹		3.85×10 ⁸	9.62×10 ⁹	6.95
NG-7 SANS at velocity selector entrance	No					
NG-C, 11×11 cm ² guide exit	Effectively	(a) 7.52×10 ⁹		2.45×10 ⁹	2.96×10 ¹¹	5.53
		(b) 7.64×10 ⁹		2.49×10 ⁹	3.01×10 ¹¹	5.51
		(c) 8.67×10 ⁹		2.88×10 ⁹	3.48×10 ¹¹	5.42
		(d) 1.57×10 ¹⁰		4.47×10 ⁹	5.41×10 ¹¹	6.29
		(e) 1.39×10 ⁹		4.48×10 ⁸	4.03×10 ¹⁰	5.56
NG-6 guide exit (6×15 cm ²) at fundamental physics station (6 in. Bi filter)	No					
NG-D at prompt gamma chemistry end station on 2×2 cm ² sample area	No	(a) 8.84×10 ⁹		2.79×10 ⁹	1.11×10 ¹⁰	5.71
		(b) 9.23×10 ⁹		2.92×10 ⁹	1.17×10 ¹⁰	5.69
		(c) 1.04×10 ¹⁰		3.34×10 ⁹	1.34×10 ¹⁰	5.62
		(d) 1.55×10 ¹⁰		4.53×10 ⁹	1.81×10 ¹⁰	6.17
		(e) 1.26×10 ⁹		3.25×10 ⁸	1.30×10 ⁹	6.95
NG-7 prompt gamma chemistry station (on 2×2 cm centered sample)	No					

The effect of $\Delta m/m=10\%$ (FWHM) in isolation (without guide misalignments) has only a marginal influence on the integrated intensities, provided that Δm is symmetrical about the nominal value. No statistically significant spectrum-integrated flux loss exceeding 1.6% is detected for any guide. In a few “favorable” configurations slight increases are observed (generally $\leq 0.5\%$).

Logically, misalignments (ii) and (iii) disfavor short wavelengths and lower m guides (such as NG-Bu and NG-BI) because the angular offsets and the “blanking angles” caused by lateral shifts are increasingly large fractions of θ_c . The smaller cross-sectional areas of these guides also maintain a relatively high number of contacts with the walls, despite the reduced θ_c . Because the misalignment losses are relatively enhanced at shorter wavelengths, the integrated

flux suffers more than the capture flux, meaning the mean transmitted wavelength increases slightly. These trends are discernable in Table III. For the approximately 60 m long guide NG-C, the cumulative misalignment errors, averaged over 20 simulations, yield a lateral displacement uncertainty of the guide exit of up to about ± 5 cm; however alignment procedures using fixed references should significantly reduce these uncertainties.

Finally, the effects of improving $R(Q)$ by decreasing the surface roughness to 0.5 nm rms. (see, e.g., Ref. 41) are estimated (for nominal value simulations). A smaller roughness gives rise to a larger relative increase in $R(Q)$ at larger Q . Therefore, if a divergence saturation occurs [such as is observed for guide NG-C for $\lambda > 5$ Å (see Sec. VI)], the

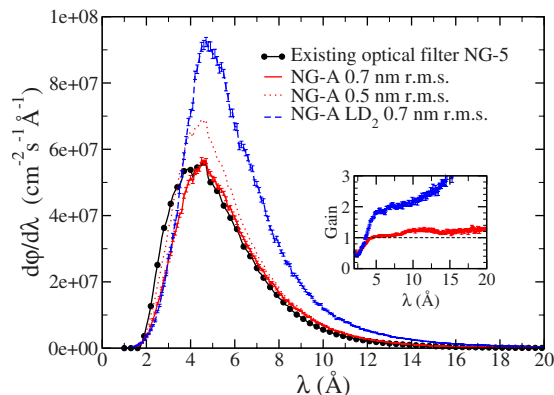


FIG. 6. (Color online) Simulated flux per unit wavelength on a 4×4 cm sample, 3.5 m downstream of the guide exit (approximately the NSE instrument configuration but with the polarizer sections replaced by regular guide sections): the curve with symbols is for the existing all- ^{58}Ni -coated optical filter guide NG-5. The solid curve without symbols is for guide NG-A with the LH_2 cold source, assuming 0.7 nm rms surface roughness and all nominal guide parameters. The dotted curve shows the estimated effect of improving the surface roughness to 0.5 nm. The dashed curve is the projected performance with a future LD_2 cold source (rms surface roughness = 0.7 nm). The error bars, where shown, are the MC statistical errors, but some symbols are omitted for clarity. The simulated intensity gains on the sample with respect to NG-5 are shown inset for the LH_2 cold source (lower curve) and the LD_2 cold source (upper curve).

relative benefits of improved roughness diminish with increasing wavelength above the saturation threshold. This is because the saturation angle corresponds to a decreasing value of Q as λ increases. A similar effect is observed at the sample position for guide NG-A, but the saturation occurs because of the collimation limitation (see Sec. V) [starting in the vertical plane for $\lambda \geq 5.0$ Å (see Table I)]. If the saturation angle magnitude is denoted by $|\alpha|$, the relative gains from decreased surface roughness are least apparent for $\lambda > 4\pi|\alpha|/Q_c^{\text{Ni}}$ when all reflections occur within the flat, low- Q , high reflectivity “Ni” portion of the supermirror reflectivity. For the SANS guides (NG-B), underillumination and reflectivity losses (and consequently trajectory angle saturation) are insignificant for wavelengths within the instrument operating ranges. Therefore, improved reflectivity produces a continuously increasing relative gain with increasing wavelength above λ_c , but such gains are modest because the majority of the coatings are already high reflectivity Ni.

In Fig. 6 simulated density functions for flux per unit wavelength $d\phi/d\lambda$ on a 4×4 cm² sample located 3.5 m downstream of the exit of guide NG-A are compared with the corresponding simulation for the ^{58}Ni -coated optical filter guide NG-5. The geometry approximates to that of a sample on the NSE instrument in each case. The results are shown with the polarizer replaced by a regular section of guide. For most operating wavelengths, the introduction of the polarizer is expected to produce a spin down beam with $d\phi/d\lambda$ about 30%–40% of the values shown in Fig. 6. For wavelengths greater than about 4 Å, the simulated intensity on sample equals or exceeds that of the existing NG-5 guide. This is partly due to the increased guide width (5 cm versus 3.5 cm for NG-5) and, for shorter wavelengths where the divergence is critical angle limited, due to the increased m

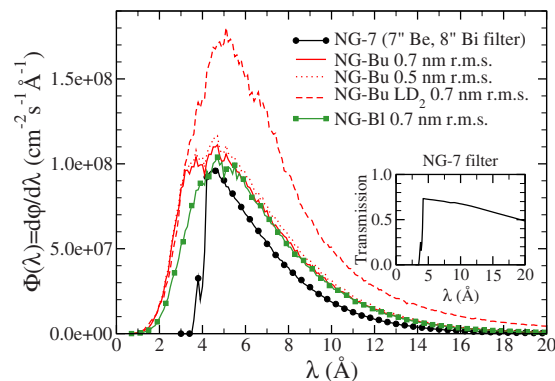


FIG. 7. (Color online) Simulated flux per unit wavelength at the velocity selector for guides NG-Bu (curves without symbols) and NG-BI (curve with square symbols) compared with the equivalent position on the existing filtered straight guide NG-7 (curve with circular symbols). The solid curves pertain to the LH_2 cold source and the dashed curve is a projection for a future LD_2 source (for guide NG-Bu), all assuming about 0.7 nm rms surface roughness. The dotted curve shows the estimated effect of improving the surface roughness to 0.5 nm for guide NG-Bu (LH_2 cold source). The beam cross sections are equal for each guide (5×5 cm²). The cooled 17.8 cm long beryllium/20.3 cm long bismuth crystal filter combination on NG-7 is assumed to have the transmission shown inset. Statistical error bars and some symbols are omitted for clarity.

(=1.8) top/bottom surface coatings. The NG-A guide exit is also slightly closer to the source by about 1.1 m. Deviations introduced by including all random imperfections reduce the integrated flux on the sample by about 3.3 ± 1.1 (1σ)% (see also Table III). The gains with a future LD_2 cold source are likely to be substantial, especially at long wavelength (see dashed curve and upper curve inset).

In Fig. 7 simulated density functions for flux per unit wavelength at the SANS velocity selector entrance positions of guides NG-BI and NG-Bu are compared with that of the existing NG-7 guide. Apart from the obvious gains of guides NG-BI and NG-Bu below the crystal filter cutoff wavelength, possibilities for significant additional gains with respect to NG-7 are limited because the beam divergence remains unchanged. Above the filter cutoff, NG-B gains are mainly attributable to the absence of crystal filter attenuation, especially for $\lambda > \lambda'$ where the PST guide transmission ideally matches that of an unfiltered straight guide with equal divergence (see Sec. III and Ref. 17). Other modest intensity gains or losses are attributable to differences in guide entrance illumination, absence of a filter gap (favoring guides NG-B), the distance of the guide exit from the source (favoring NG-7 by about -3.7 m with respect to NG-Bu and by about -7.4 m with respect to NG-BI), and differences in $R(Q)$. Deviations introduced by including all random imperfections reduce the integrated guide exit flux by about 6.2 ± 0.5 (1σ)% for NG-Bu and by 7.2 ± 0.8 (1σ)% for NG-BI (see also Table III).

In Fig. 8 simulated density functions for neutrons per second per unit wavelength at the NG-C guide exit are compared with those of the existing straight guide NG-6, also used for fundamental physics experiments. Three configurations for NG-6 are shown. By comparing neutrons per second, these data account for the $\sim 34\%$ increase in the beam size at the NG-C guide exit (11×11 cm²), compared with

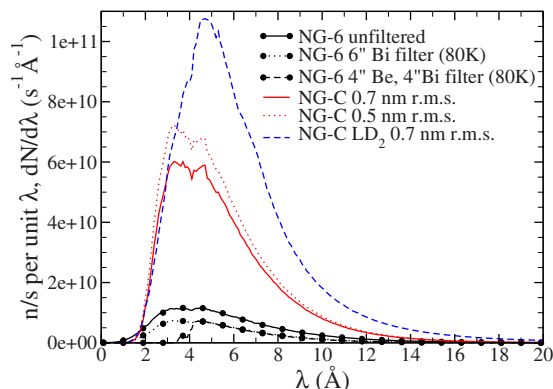


FIG. 8. (Color online) Simulations of neutrons per second per unit wavelength at the exits of guide NG-C (curves without symbols) and the existing guide NG-6 (curves with symbols). For NG-C, the solid and dashed curves show the projected performance with the LH₂ cold source and a future LD₂ cold source, respectively, both assuming about 0.7 nm rms surface roughness and nominal guide parameters. The dotted curve shows the estimated effect of improving the surface roughness to 0.5 nm rms with the LH₂ source for guide NG-C. The three configurations shown for NG-6 (all with the LH₂ cold source) are unfiltered beam (solid curve with symbols), with a cooled 15.2 cm quasisingle crystal bismuth gamma filter (dotted curve with symbols), and with a cooled 10.2 cm beryllium/10.2 cm bismuth filter combination (dashed curve with symbols). Statistical error bars and some symbols are omitted for clarity.

6 cm(*w*) × 15 cm(*h*) for NG-6. The integrated data in Table III suggest that the total neutrons per second at the guide exit could be about 7.5 times greater for NG-C than at NG-6 with a 15.2 cm bismuth filter (which is probably the fairest comparison). With a future LD₂ cold source, this factor could increase to about 13 or possibly more. Deviations introduced by including all random imperfections reduce the integrated guide exit flux by about 1.8 ± 0.5 (1σ)% and the capture flux by about 1.6 ± 0.4 (1σ)% (see also Table III).

In Fig. 9 simulated density functions for capture flux per unit wavelength on a centrally placed 2×2 cm² sample area located about 39 cm downstream of the exit of guide NG-D are compared with that at the existing PGAA station on guide NG-7. (The sample size and distance from the guide exit correspond to the current NG-7 PGAA configuration). The integrals of these curves (see Table III) suggest that a capture flux gain factor of around 7 or more is anticipated, increasing to around 12 with a LD₂ cold source. The substantial gain is largely attributable to the use of significantly higher critical angle coatings and focusing for guide NG-D, contrasting with the nonfocusing, all-⁵⁸Ni-coated NG-7 guide setup. Deviations introduced by including all random imperfections reduce the integrated flux on sample by about 4.6 ± 1.0 (1σ)% and the capture flux by about 4.2 ± 0.7 (1σ)%.

VIII. CONCLUSIONS

The guide designs for the NCNR expansion project are customized, wherever possible, to suit the instrument requirements. This involves optimizing the intensity within the instrument divergence limits and operating wavelength range, while minimizing divergent beam components not reaching the sample. Curving the guides initially allows an increased number of beams to be extracted from a restricted

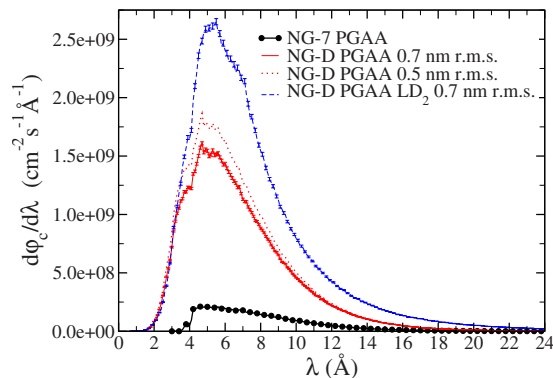


FIG. 9. (Color online) Simulated capture flux per unit wavelength at the sample position of the existing PGAA station on NG-7 (curve with symbols) compared with that at the end-guide position of NG-D for the existing LH₂ cold source (solid curve) and for the projected LD₂ cold source (dashed curve), assuming about 0.7 nm rms surface roughness. The dotted curve shows the estimated effect of improving the surface roughness to 0.5 nm rms with the LH₂ cold source for guide NG-D. The sample size is assumed to be 2×2 cm², centrally placed at about 39 cm from the guide exit. The error bars shown are the MC statistical errors, but some symbols are omitted for clarity.

beam tube and also excludes direct lines of sight between the source and the instruments, reducing or eliminating the need for crystal filters. Consequently, some of the transmission disadvantages of curved guides with respect to equivalent straight guides are offset and the unfiltered curved guide outperforms the filtered straight guide at longer wavelengths in some instances. Acceptance diagram principles applied to idealized curved-straight approximations to the actual guides yield initial estimates of fundamental guide characteristics, but are of limited use for optimization or accurate performance estimates of the real device. For this purpose MC simulations have been performed in order to fully account for departures from idealized geometry, reflectivity, and illumination. Having identified high performance and viable guide geometries, a final phase of MC simulations was conducted in order to restrict the supermirror *m* only to what usefully enhances the intensity at the sample. Attention to this final step has resulted in significantly improved performance-cost effectiveness of the high flux guides, in particular.

IX. DISCLAIMER

Certain trade names and company products are identified in order to specify adequately the experimental procedure. In no case does such identification imply recommendation or endorsement by the National Institute of Standards and Technology, nor does it imply that the products are necessarily the best for the purpose.

ACKNOWLEDGMENTS

Helpful discussions with a number of colleagues, especially David Mildner, Alan Heald, Don Pierce, Charles Majkrzak, Dan Neumann, John Copley, and Peter Böni are gratefully acknowledged. The author also wishes to thank David Mildner and Charles Glinka for their critical reading of this manuscript.

- ¹P. A. Egelstaff, H. London, and F. J. Webb, Proceedings of the Conference de Physique des Basses Températures, Paris, 1955, p. 375 (unpublished).
- ²J. Christ and T. Springer, *Nukleonik* **4**, 23 (1962).
- ³H. Maier-Leibnitz and T. Springer, *J. Nucl. Energy, Parts A/B* **17**, 217 (1963).
- ⁴R. E. Williams and J. M. Rowe, *Physica B* **311**, 117 (2002).
- ⁵M. Monkenbusch, R. Schätzler, and D. Richter, *Nucl. Instrum. Methods Phys. Res. A* **399**, 301 (1997).
- ⁶N. Rosov, S. Rathgeber, and M. Monkenbusch, in *Scattering from Polymers: Characterization by X-rays, Neutrons, and Light*, edited by P. Cebe, B. S. Hsaio, and D. J. Lohse, ACS Symposium Series, Vol. 739 (American Chemical Society, Washington D.C., 2000), pp. 103–116.
- ⁷C. J. Glinka, J. Barker, B. Hammouda, S. Krueger, J. Moyer, and W. Orts, *J. Appl. Crystallogr.* **31**, 430 (1998).
- ⁸J. A. Dura, D. J. Pierce, C. F. Majkrzak, N. C. Maliszewskij, D. J. McGillivray, M. Lösche, K. V. O'Donovan, M. Mihailescu, U. Perez-Salas, D. L. Worcester, and S. H. White, *Rev. Sci. Instrum.* **77**, 074301 (2006).
- ⁹R. M. Lindstrom, *J. Res. Natl. Inst. Stand. Technol.* **98**, 127 (1993).
- ¹⁰R. G. Downing, G. P. Lamaze, J. K. Langland, and S. T. Hwang, *J. Res. Natl. Inst. Stand. Technol.* **98**, 109 (1993).
- ¹¹K. Andersen, H. Ballhausen, D. Bazzoli, J. Beaucour, P. Böni, L. Didier, E. Farhi, R. Gähler, T. Hürlimann, C. Ruget, and I. Sutton, Proceedings of the International Symposium on Research Reactor and Neutron Science-In Commemoration of the 10th Anniversary of HANARO, Daejeon, Korea, April 2005 (unpublished).
- ¹²E. Steichele and C. Schanzer, Proceedings of the 8th meeting of the International Group on Research Reactors, Munich, Germany, April 2001 (unpublished).
- ¹³Y. Kawabata, M. Suzuki, H. Takahashi, N. Onishi, A. Shimanuki, Y. Sugawa, N. Niino, T. Kasai, K. Funasho, S. Hayakawa, and K. Okuhata, *J. Nucl. Sci. Technol.* **27**, 1138 (1990).
- ¹⁴C. J. Carlile, M. W. Johnson, and W. G. Williams, *Neutron Guides on Pulsed Sources* (Rutherford Laboratory, Chilton, Didcot, Oxon, 1979).
- ¹⁵D. F. R. Mildner, *Nucl. Instrum. Methods Phys. Res. A* **290**, 189 (1990).
- ¹⁶J. R. D. Copley and D. F. R. Mildner, *Nucl. Sci. Eng.* **110**, 1 (1992).
- ¹⁷D. F. R. Mildner and J. C. Cook, *Nucl. Instrum. Methods Phys. Res. A* **592**, 414 (2008).
- ¹⁸I. Anderson, *Proc. SPIE* **1738**, 118 (1992).
- ¹⁹V. F. Turchin, *At. Energy Rev.* **22**, 119 (1967).
- ²⁰B. P. Schoenborn, D. L. D. Caspar, and O. F. Kammerer, *J. Appl. Crystallogr.* **7**, 508 (1974).
- ²¹F. Mezei, *Commun. Phys. (London)* **1**, 81 (1976).
- ²²J. B. Hayter and H. A. Mook, *J. Appl. Crystallogr.* **22**, 35 (1989).
- ²³P. Böni, personal communication (May 2007).
- ²⁴Ch. Rehm, M. Agamalian, and F. Klose, "Neutron Supermirrors: Design and Application," Oak Ridge National Laboratory, Spallation Neutron Source Project, May 2002.
- ²⁵J. R. D. Copley, *Nucl. Instrum. Methods Phys. Res. A* **355**, 469 (1995).
- ²⁶A. Schirmer and D. F. R. Mildner, *Meas. Sci. Technol.* **2**, 1059 (1991).
- ²⁷D. F. R. Mildner, *Nucl. Instrum. Methods Phys. Res. A* **292**, 693 (1990).
- ²⁸D. F. R. Mildner and B. Hammouda, *J. Appl. Crystallogr.* **25**, 39 (1992).
- ²⁹D. Dubbers, *Nucl. Instrum. Methods Phys. Res. A* **349**, 302 (1994).
- ³⁰J. C. Cook and J. R. D. Copley, *Rev. Sci. Instrum.* **75**, 430 (2004).
- ³¹MCNP—A General Monte Carlo N-Particle Transport Code, Version 5, X-5 Monte Carlo Team, Diagnostics Applications Group, Los Alamos National Laboratory.
- ³²R. E. Williams, personal communication (July 2006).
- ³³F. Mezei, *J. Neutron Res.* **6**, 3 (1997).
- ³⁴C. Schanzer, P. Böni, U. Filges, and T. Hils, *Nucl. Instrum. Methods Phys. Res. A* **529**, 63 (2004).
- ³⁵G. E. Granroth, D. H. Vandergriff, and S. E. Nagler, *Physica B* **385**, 1104 (2006).
- ³⁶P. Böni, *Nucl. Instrum. Methods Phys. Res. A* **586**, 1 (2008).
- ³⁷S. Mühlbauer, P. G. Niklowitz, M. Stadlbauer, R. Georgii, P. Link, J. Stahn, and P. Böni, *Nucl. Instrum. Methods Phys. Res. A* **586**, 77 (2008).
- ³⁸D. F. R. Mildner, personal communication (July 2006).
- ³⁹F. Samuel, B. Farnoux, B. Ballot, and B. Vidal, *Proc. SPIE* **1738**, 54 (1992).
- ⁴⁰P. Böni, personal communication (July 2007).
- ⁴¹Schott Advanced Optics Newsletter, Vol. III, No. 1, January 2008.
- ⁴²J. R. D. Copley and J. C. Cook, *Physica B* **283**, 386 (2000).
- ⁴³P. Allenspach, P. Böni, and K. Lefmann, *Proc. SPIE* **4509**, 157 (2001).